Table S1 (related to Figure 3)
Model refinement and validation statistics

Model #	**Model 1**	**Model 2**	**Model 3**	**Model 4**	**Model 5**	**Model 6**	**Model 7**
Branch 1 position	E11	E11 anti-	E11	E11	E11	E11 anti-	E11
Polarity	parallel	parallel	parallel	parallel	parallel	parallel	anti-parallel
Branch 2 position			E9	E9 anti-	E8 anti-	E12	E8
Polarity			parallel	parallel	parallel	parallel	parallel
							3-chain overlap high clash score not compatible
Model composition							
Nonhydrogen atoms	13,992	14,010	14,010	14,042	14,054	14,050	14,019
Protein residues	1,871	1,873	1,873	1,877	1,878	1,878	1,874
Ligands	5 Mg^{2+} 6 ATP	5 Mg^{2+} 6 ATP	5 Mg^{2+} 6 ATP	5 Mg^{2+} 6 ATP	5 Mg^{2+} 6 ATP	5 Mg^{2+} 6 ATP	5 Mg^{2+} 6 ATP
R.m.s. deviations							
Bond lengths (Å)	0.006	0.005	0.006	0.006	0.006	0.006	0.006
Bond angles (°)	1.162	1.143	1.452	1.449	1.465	1.457	1.440
Validation							
MolProbity score	1.82	1.67	1.69	1.70	1.80	1.67	1.72
Clashscore	4.53	3.76	3.80	3.86	4.15	3.42	4.38
Clashscore pore	0.00	0.00	0.00	0.00	0.00	0.00	20.12
Poor rotamers (%)	1.57	1.19	1.27	1.26	1.64	1.34	1.19
Ramachandran plot							
Favored (%)	93.11	93.07	93.11	93.07	93.18	93.08	93.00
Allowed (%)	6.78	6.93	6.84	6.88	6.71	6.87	6.94
Disallowed (%)	0.11	0.05	0.05	0.05	0.11	0.05	0.05

Model statistics for the katanin hexamer bound to polyglutamylated tails added at different positions in the β-tubulin tail. The positions of the poly-Glu branches on the tubulin tail are indicated for each model. Branches with the same polarity as the tail peptide are labelled as parallel, with the opposite polarity, anti-parallel. The katanin hexamer bound to a single substrate peptide was used as the starting model (PDBID 6UGD)[53] (Figure S4B). VPS4 bound to cyclic peptide (PDB ID 6OO2) was used as a guide to position the backbone of a branch within the pore [114]. **Model 1** has one parallel poly-Glu branch, six residues long (spanning to the end of the pore), at position 11 of the tail (Figs. 3F and S4C); **Model 2** has one anti-parallel poly-Glu branch, eight residues long (spanning to the end of the pore), at position 11 of the tail (Figure S4D). **Model 3** has one parallel poly-Glu branch, six-residues long at position 11, and a second parallel poly-Glu branch, 2 residues long at position 9 (Figures 3G left panel and S4E). We note that longer branches can be accommodate at position 9 because they can escape the confines at the pore beyond the first 3 residues. **Model 4** has one parallel poly-Glu branch at position 11 and a second anti-parallel poly-Glu branch at position 9, both six residues long, (Figures 3H middle panel, S4F). **Model 5** has one parallel poly-Glu branch, 6 residues long, at position 11, and a second anti-parallel poly-Glu branch, seven residues long, at position 8 (Figures 3H middle panel, S4G). **Model 6** has an anti-parallel poly-Glu branch, eight residues long, at position 11, and a second parallel branch, five residues at position 12 (Figures 3H middle panel, S4H). **Model 7** has one anti-parallel poly-Glu branch, eight-residues long, at position 11, and second parallel branch, one residue long at position 8 (Figures 3G, third panel from the left; S4I) that clashes with pore loop residues.

Figure S1 (related to Figure 1).

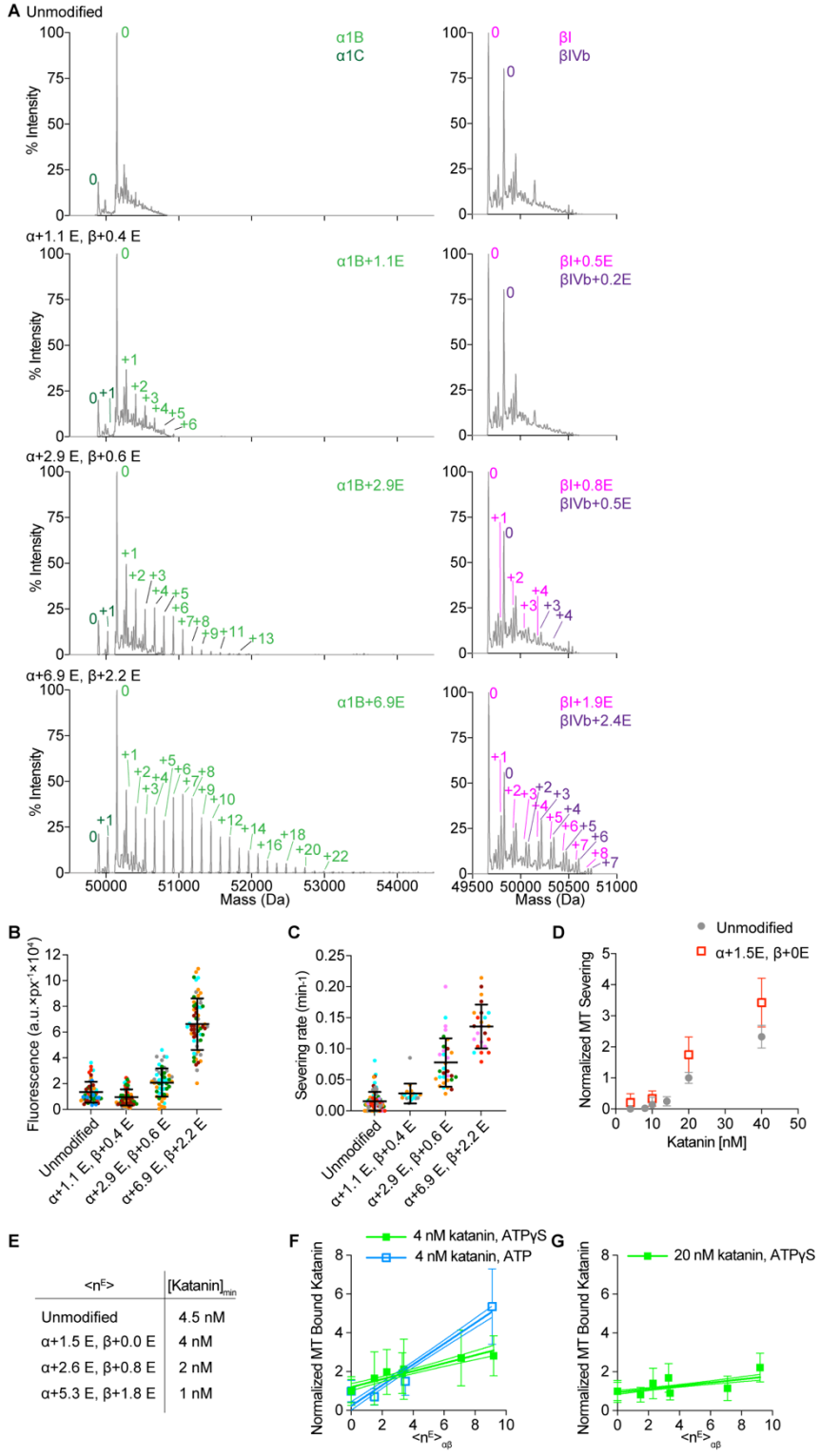

Mass spectra, binding, and activity on TTLL6 modified microtubules.

(**A**) Reversed phase LC-MS spectra of microtubules glutamylated by TTLL6 and used in assays shown in Figure 1. Throughout, numbers of glutamates added to α- and β-tubulin are shown in green and magenta/purple, respectively. The weighted mean of glutamates $\langle n^E \rangle$ added to α- and β-tubulin (overall and for the separate isoforms) are denoted $\alpha + \langle n^E \rangle_\alpha$ and $\beta + \langle n^E \rangle_\beta$, respectively.

(**B**) Background-corrected fluorescence of katanin bound to microtubules with different glutamylation levels introduced by TTLL6 (normalized data shown in Figure 1B). Different chambers from different days shown in different colors. Error bars, mean and S. D.

(**C**) Non-normalized severing rates of microtubules with different glutamylation levels introduced by TTLL6 s (normalized data shown in Figure 1E). Different chambers from different days shown in different colors. Error bars, mean and S. D.

(**D**) Severing as a function of katanin concentration for unmodified microtubules and microtubules glutamylated by TTLL6.

(**E**) Minimum katanin concentration required to see one microtubule break over a total period of ten minutes for microtubules with different glutamylation levels introduced by TTLL6 (see STAR Methods).

(**F**) Katanin recruitment to the microtubule at 4 nM in the presence of ATP (blue) and ATPγS (green) as a function of TTLL6 glutamylation; $n \geq 31$ microtubules for each condition from multiple chambers. Lines, linear regression and 95% confidence interval.

(**G**) Katanin recruitment to the microtubule at 20 nM in the presence of ATPγS as a function of TTLL6 glutamylation; $n \geq 31$ microtubules for each condition. Lines, linear regression and 95% confidence interval.

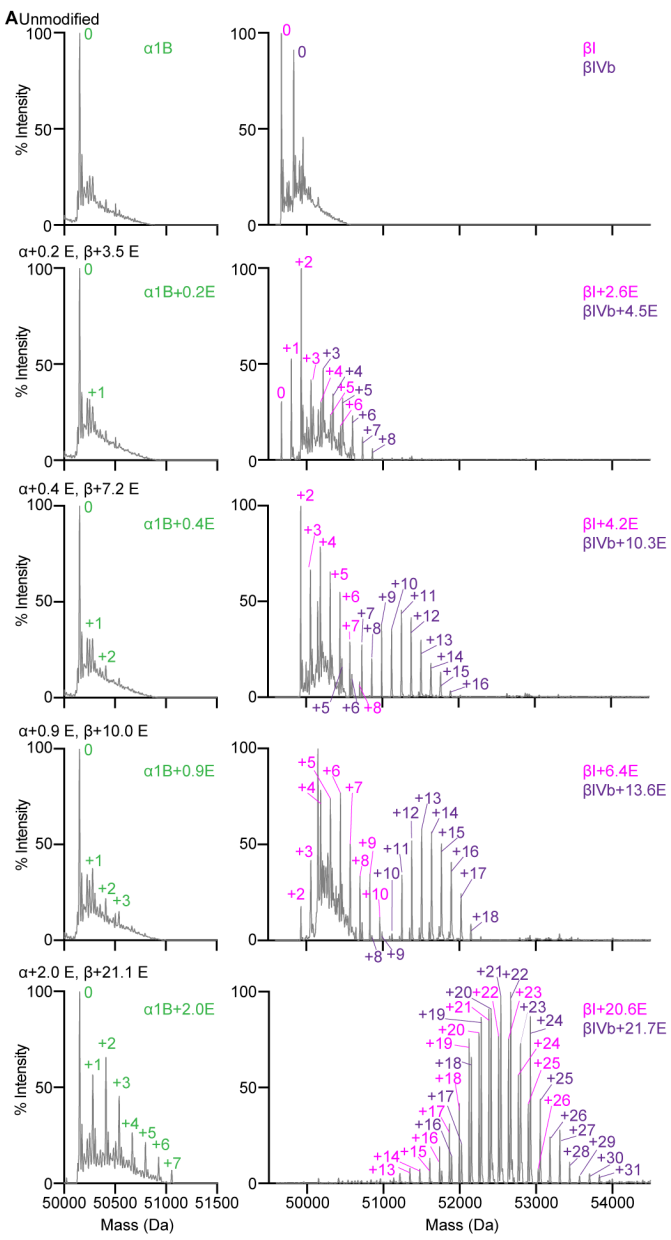

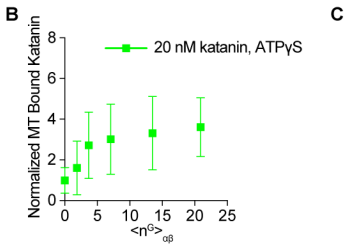

C

<n^E>	[Katanin]$_{min}$
Unmodified	4.5 nM
α+0 E, β+1.4 E	3.5 nM
α+0.2 E, β+3.2 E	4.5 nM
α+0.3 E, β+5.7 E	4.5 nM
α+0.9 E, β+10.3 E	4.5 nM
α+2.5 E, β+18.5 E	5.5 nM

Figure S2 (related to Figure 2). Mass spectra, binding, and activity on TTLL7 modified microtubules.

(**A**) Reversed phase LC-MS spectra of microtubules glutamylated by TTLL7 and used in assays shown in Figure 2. Throughout, numbers of glutamates added to α- and β-tubulin are shown in green and magenta/purple, respectively. The weighted mean of glutamates $\langle n^E \rangle$ added to α- and β-tubulin (overall and for the separate isoforms) are denoted $\alpha + \langle n^E \rangle_\alpha$ and $\beta + \langle n^E \rangle_\beta$, respectively.

(**B**) Katanin recruitment to the microtubule at 20 nM in the presence of ATPγS as a function of TTLL7 glutamylation; Error bars, mean and S. D. $n \geq 68$ microtubules for each condition.

(**C**) Minimum katanin concentration required to see one microtubule break over a total period of ten minutes for microtubules with different glutamylation levels introduced by TTLL7 (also see STAR Methods).

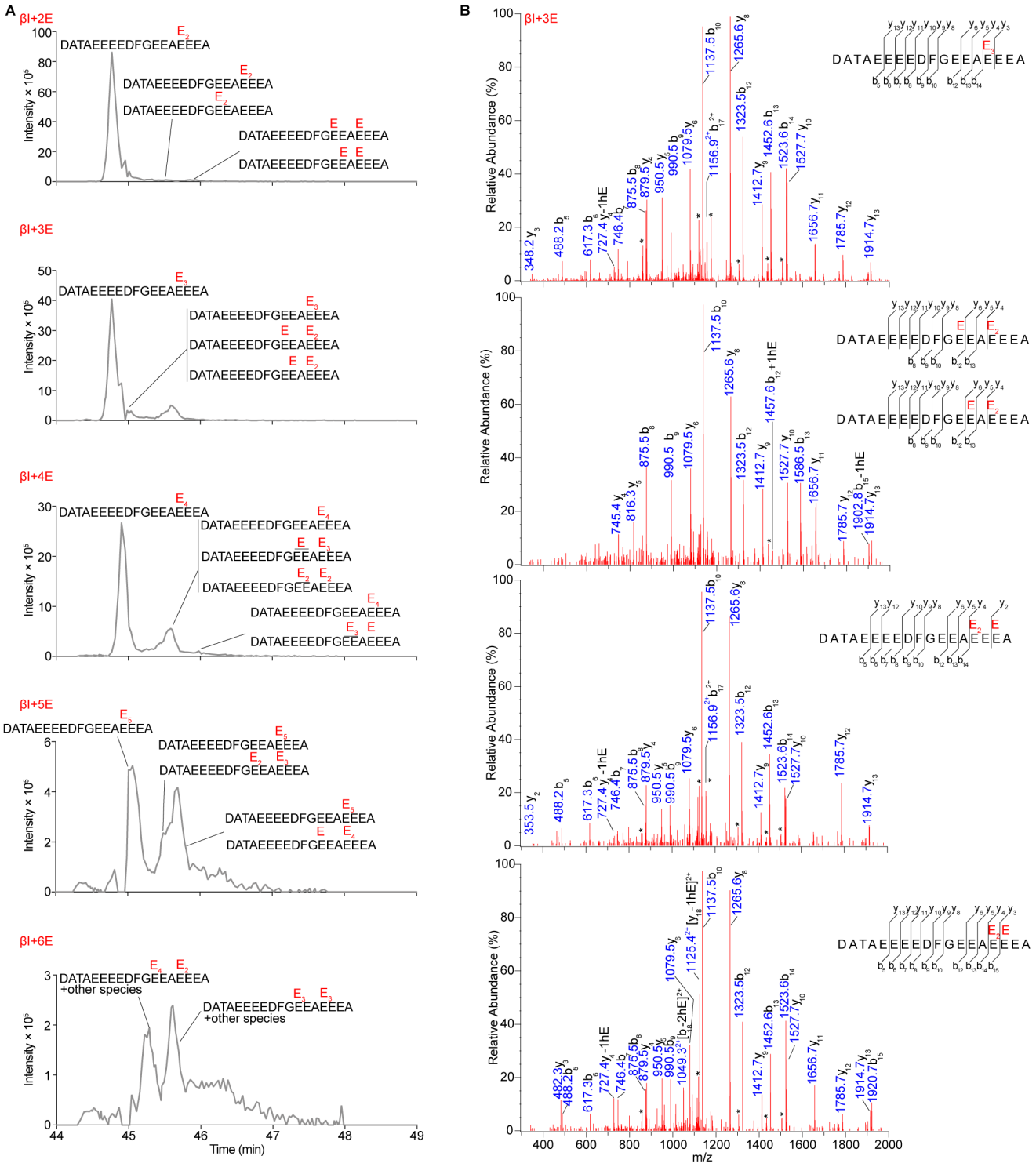

Figure S3 (related to Figure 3).
MS/MS analysis of glutamylated tubulin tails

(**A**) XIC of βI-tubulin tail peptides released from microtubules glutamylated by TTLL7, showing the distribution of peptides with different glutamylation patterns for β-tubulin tails with 2, 3, 4, 5 and 6 glutamates.

(**B**) Subset of MS/MS sequencing data of βI-tubulin tails glutamylated by TTLL7. Individual b-, and y-series ions and the amino acid sequence for each spectrum are indicated. m/z values of the peaks are shown in blue. Asterisks indicate ions with a neutral loss of a water molecule.

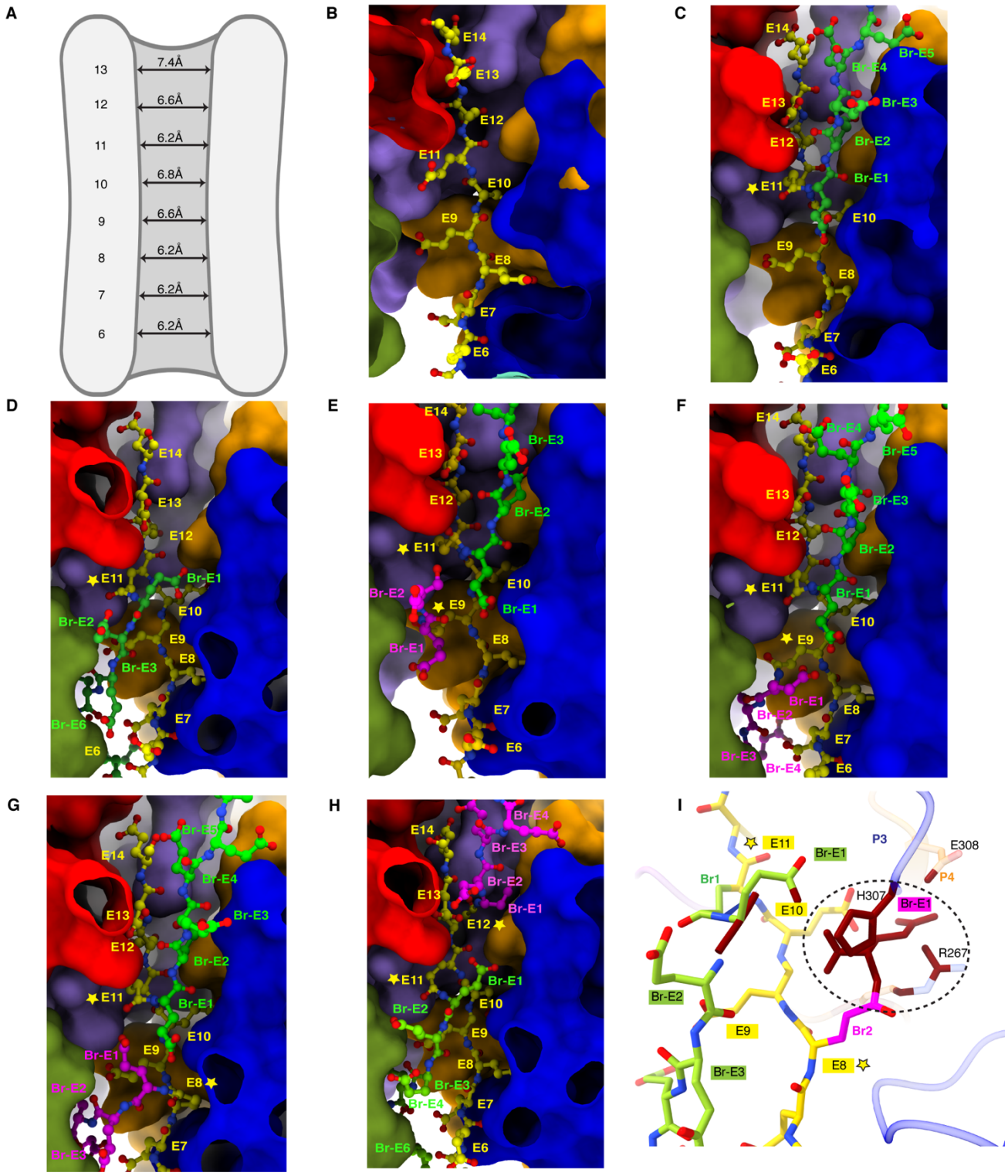

Figure S4 (related to Figure 3).
Accommodation of diverse glutamate branch structures by the katanin pore, and restrictions
(**A**) Schematic of the katanin central pore showing pore dimensions at positions along the tubulin tail, indicated on the left. Residues 1 through 5 and residue 14 of the tail are outside the pore. Measurements were performed manually in UCSF Chimera[146] and automatically using MOLEonline[149] and gave similar values.
(**B-H**). Katanin pore bound to tubulin tails with various glutamate branch configurations; protomers P1 through P6 colored as P1 green, P2 turquoise, P3 blue, P4 orange, P5 purple, P6 red. Tubulin tail, yellow ball-and-stick representation; unmodified tubulin tail (PDBID 6UGD)[53], (B); tubulin tail functionalized with a parallel six-

residue glutamate branch starting at E11, green (Model 1, Table S1, Figure 3F). Branch point highlighted with yellow star, branch glutamates, labeled Br-E, (C); tubulin tail with an anti-parallel eight-residue glutamate branch starting at E11, green (Model 2, Table S1), (D); tubulin tail with a parallel six-residue glutamate branch starting at E11, green, and a parallel two-residue glutamate branch starting at E9, magenta (Model 3, Table S1, Figure 3G, left panel), (E); tubulin tail with a parallel six-residue-long branch starting at E11, green, and an anti-parallel six-residue glutamate branch starting at E9, magenta (Model 4, Table S1, Figure 3H middle panel),(F); tubulin tail with a parallel six-residue glutamate branch starting at E11, green, and an anti-parallel seven-residue glutamate branch starting at E8, magenta (Model 5, Table S1, Figure 3H middle panel), (G); tubulin tail with an anti-parallel eight-residue glutamate branch starting at E11, green, and parallel five-residue glutamate branch starting at E12, magenta (Model 6, Table S1, Figure 3H middle panel), (H); A glutamylated tail peptide with two juxtaposed branches, creating a three-peptide-wide substrate produces severe clashes (I). Tubulin tail, yellow, the first branch, Br1, green, starts at position E11 in the tubulin tail and runs anti-parallel to the tail; the second branch, Br2, magenta, starts at E8 of the tail, runs parallel to the tail and clashes with katanin pore loop residues in protomers P3 and P4. Atoms that clash with Br2-E1 are in maroon and highlighted by a dashed ellipse (Model 7, Table S1, Figure 3G, third from left).

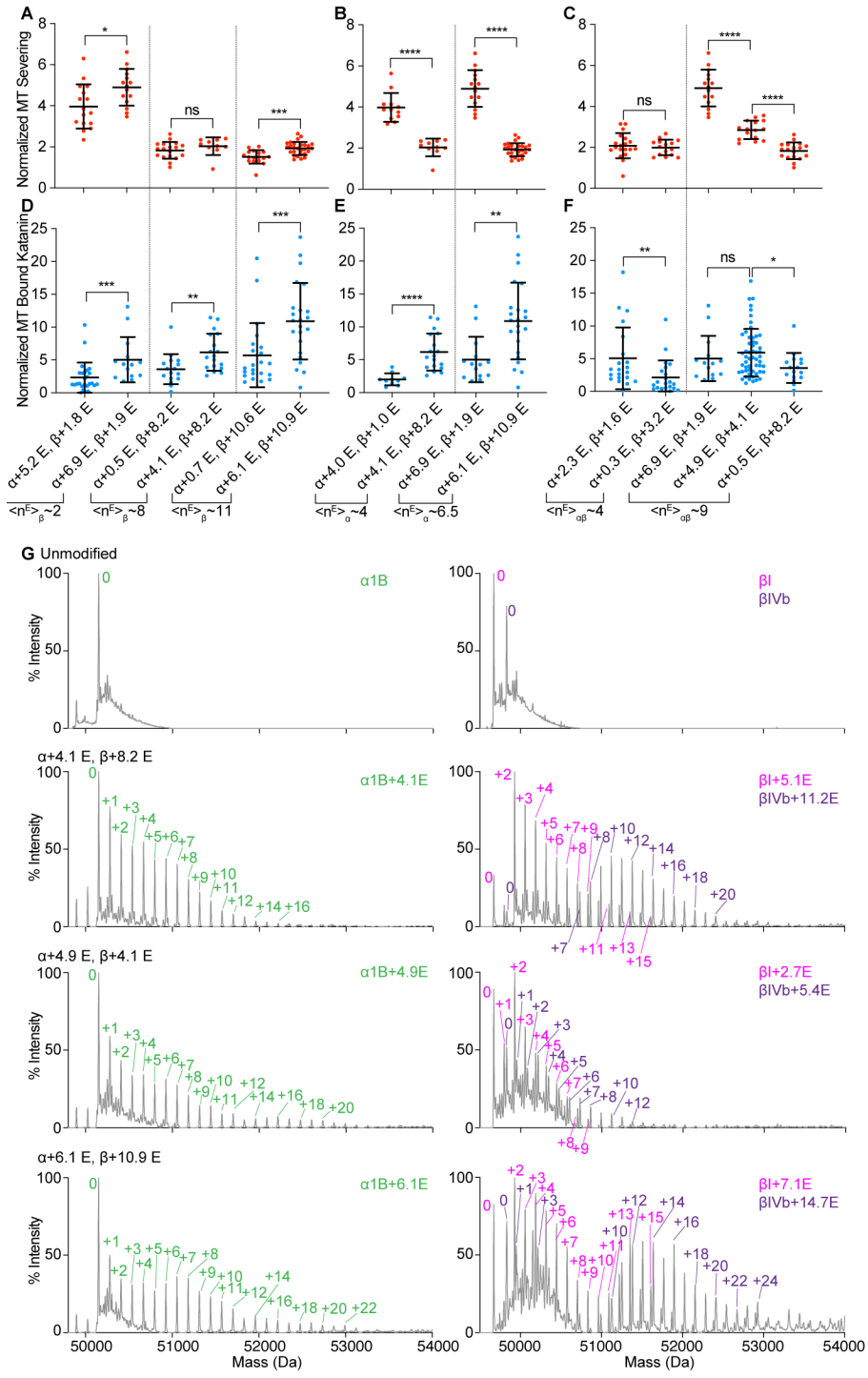

Figure S5 (related to Figure 4).

Combinatorial regulation by α- and β-tubulin glutamylation

(**A-C**) Severing of microtubules with similar $\langle n^E \rangle$ on β-tubulin and varying $\langle n^E \rangle$ on α-tubulin (A), similar $\langle n^E \rangle$ on α-tubulin and varying $\langle n^E \rangle$ on β-tubulin (B), and similar $\langle n^E \rangle$ on the αβ-tubulin dimer (C), normalized to that of unmodified microtubules. Reactions performed with 20 nM katanin and 1 mM ATP; n ≥ 10 microtubules for each condition from multiple chambers. Error bars, S.D. p-value > 0.05 (ns), ≤ 0.05 (*), 0.01 (**), 0.001 (***), 0.0001 (****) by 2-tailed t-test or Mann-Whitney test.

(**D-F**) Katanin levels recruited to microtubules with similar $\langle n^E \rangle$ on β-tubulin and varying $\langle n^E \rangle$ on α-tubulin (D), similar $\langle n^E \rangle$ on α-tubulin and varying $\langle n^E \rangle$ on β-tubulin (E), and similar $\langle n^E \rangle$ on the αβ-tubulin dimer (F), normalized to that of unmodified microtubules; n ≥ 10 microtubules for each condition from multiple chambers.

Reactions performed with 4 nM katanin and 1 mM ATP; Error bars, S.D. p-value > 0.05 (ns), ≤ 0.05 (*), 0.01 (**), 0.001 (***), 0.0001 (****) by 2-tailed t-test or Mann-Whitney test.

(**G**) Reversed phase LC-MS spectra of microtubules glutamylated by TTLL6 and 7 and used in assays shown in Figure 4. Throughout, numbers of glutamates added to α- and β-tubulin are shown in green and magenta/purple, respectively. The weighted mean of glutamates $\langle n^E \rangle$ added to α- and β-tubulin (overall and for the separate isoforms) are denoted $\alpha + \langle n^E \rangle_\alpha$ and $\beta + \langle n^E \rangle_\beta$, respectively.

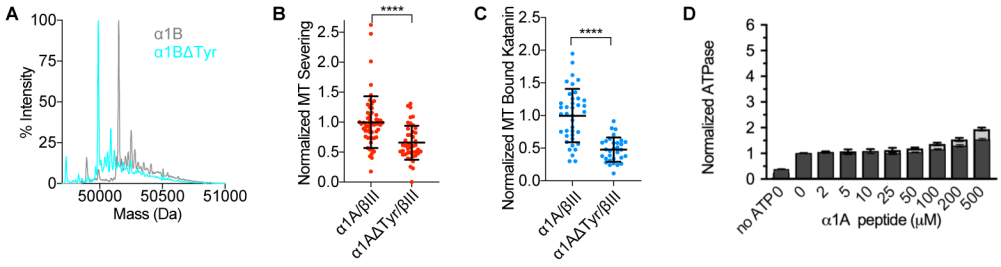

Figure S6 (related to Figure 5).

Mass spectra of tyrosinated and detyrosinated tubulin and effects of detyrosination on microtubule binding and katanin ATPase

(A) Reversed phase LC-MS spectra of unmodified (grey) and detyrosinated (cyan) α-tubulin.

(B) Rate of severing of recombinant human unmodified tyrosinated (α1A/βIII) microtubules and detyrosinated microtubules (α1AΔTyr/βIII), normalized to tyrosinated (α1A/βIII) microtubules; Reactions performed at 20 nM katanin and 1 mM ATP; n = 56, 44 unmodified and detyrosinated microtubules, respectively. Error bars, S. D. $p \leq 0.0001$ (****) by 2-tailed t-test or Mann-Whitney test.

(C) Katanin bound to recombinant human unmodified tyrosinated (α1A/βIII) microtubules and detyrosinated microtubules (α1AΔTyr/βIII), normalized to tyrosinated (α1A/βIII) microtubules; Reactions performed at 4 nM katanin and 1 mM ATP; n = 39, 31 unmodified and detyrosinated microtubules, respectively. Error bars, S. D. $p \leq 0.0001$ (****) by 2-tailed t-test or Mann-Whitney test.

(D) ATPase activity of katanin p60 with tyrosinated (VDSVEGEGEEEGEEY; light grey bars) and detyrosinated (VDSVEGEGEEEGEE; dark grey bars) peptides at the indicated concentrations; n=4. Error bars, S.E.M.

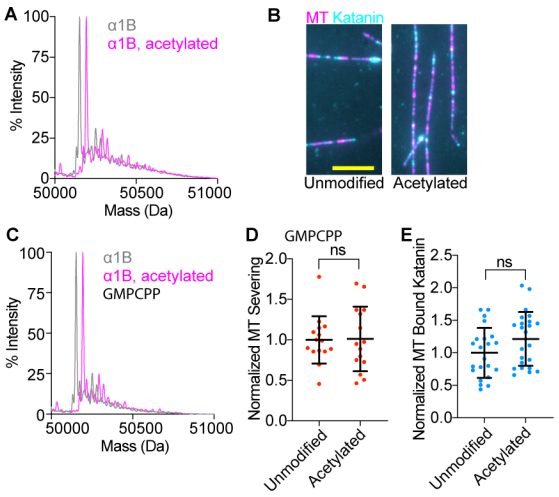

Figure S7 (related to Figure 6).

Mass spectra of acetylated tubulin and effects of acetylation on microtubule binding and severing.

(A) Reversed phase LC-MS spectra of unmodified (grey) and acetylated (magenta) α-tubulin.

(**B)** Micrographs showing Atto488-labeled katanin bound to unmodified and acetylated microtubules; Reactions performed at 4 nM katanin with 1 mM ATP; Scale bar, 5 μm.

(**C**) Reversed phase LC-MS spectra of unmodified (grey) and acetylated (magenta) α-tubulin in GMPCPP stabilized microtubules

(D) Rate of severing of unmodified and acetylated GMPCPP-stabilized microtubules, normalized to unmodified microtubules. Reactions performed at 20 nM katanin with 1 mM ATP; n = 15, 15 unmodified and acetylated microtubules, respectively from multiple chambers. Error bars, S. D. $p > 0.05$ (ns) by 2-tailed t-test.

(E) Katanin bound to unmodified and acetylated GMPCPP-stabilized microtubules, normalized to unmodified microtubules. Reactions performed at 4 nM katanin with 1 mM ATP; n = 22, 23 unmodified and acetylated microtubules, respectively from multiple chambers. Error bars, S. D. $p > 0.05$ (ns) by 2-tailed t-test.

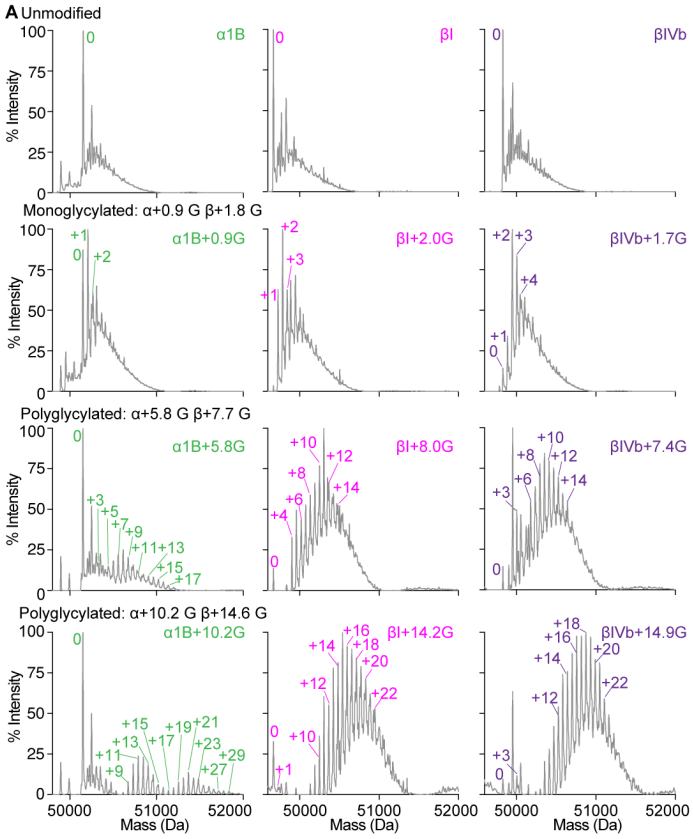

Figure S8 (related to Figure 7)
Mass spectra of glycylated microtubules.
Reversed phase LC-MS spectra of microtubules glycylated by TTLL3 and 10 and used in assays shown in Figure 7. Throughout, numbers of glycines added to α- and β-tubulin are shown in green and magenta/purple, respectively. The weighted mean of glycines $\langle n^G \rangle$ added to α- and β-tubulin (overall and for the separate isoforms) are denoted $\alpha + \langle n^G \rangle_\alpha$ and $\beta + \langle n^G \rangle_\beta$, respectively.

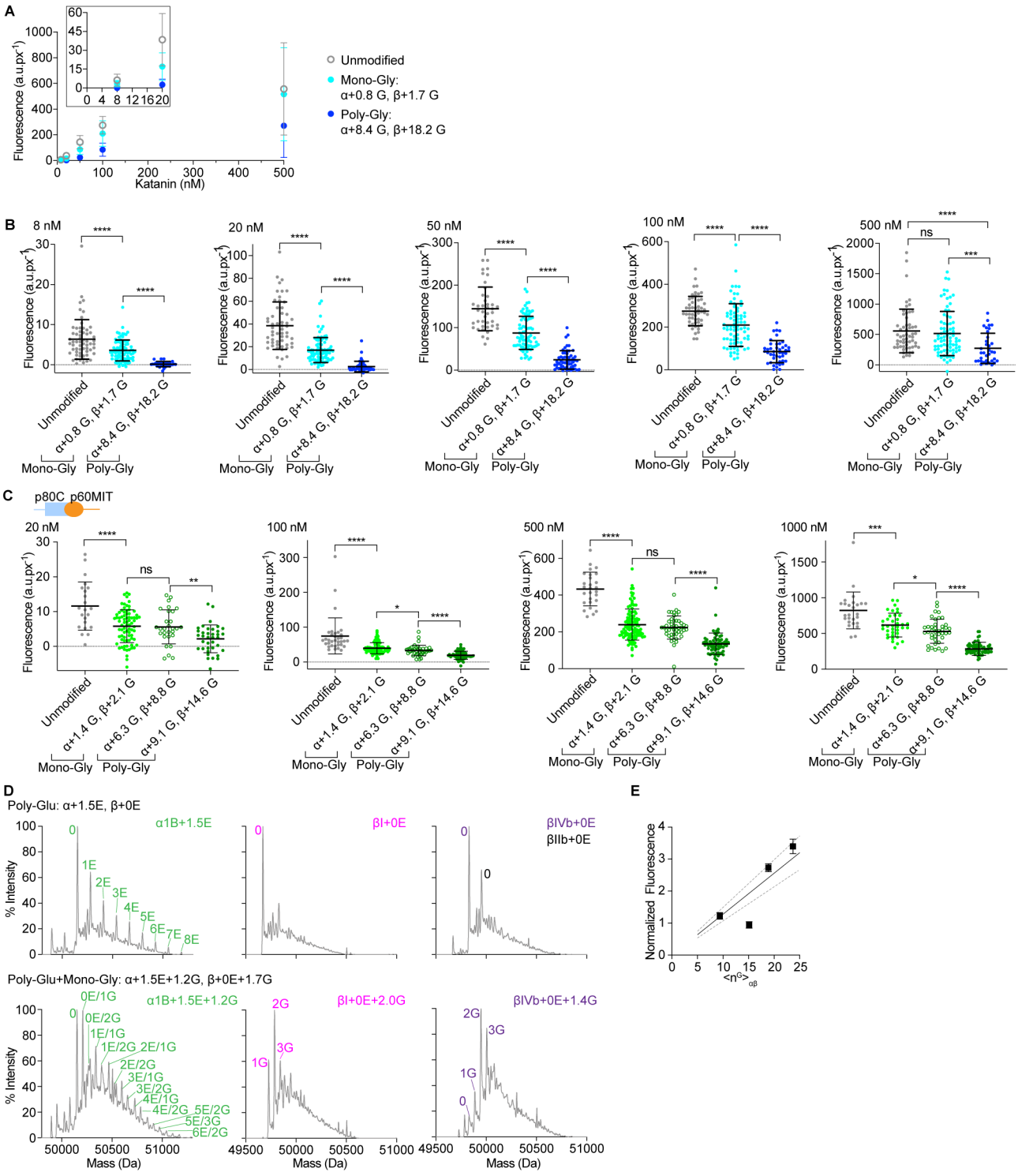

Figure S9 (related to Figure 7).
Binding to glycylated microtubules and LC-MS of glutamylated mono-glycylated microtubules.
(A) Background-corrected fluorescence intensity of Atto-488 labeled katanin bound to microtubules with different glycylation levels as a function of katanin concentration, in the presence of 1 mM ATPγS; Glycylation levels shown on the right; Microtubules were modified with TTLL3 (mono-Gly) and TTLL3+TTLL10 (poly-Gly); weighted mean of glycines $\langle n^G \rangle$ added to α- and β-tubulin are denoted $\alpha + \langle n^G \rangle_\alpha$ and $\beta + \langle n^G \rangle_\beta$, respectively; $n \geq 32$ microtubules for each condition; Mean and S.D. Inset shows binding at 8 and 20 nM katanin concentrations.

(B) Scatter plots of data shown in (A) at indicated katanin concentrations. Mean and S.D; p-value > 0.05 (ns), ≤ 0.05 (*), 0.01 (**), 0.001 (***), 0.0001 (****) by two-tailed t-test.
(C) Background-corrected fluorescence intensity of Atto-488 labeled p60ΔAAA/p80Cterm katanin bound to microtubules with different glycylation levels (plots shown in Figure 7G). The weighted mean of glycines $\langle n^G \rangle$ added to α- and β-tubulin are denoted $\alpha + \langle n^G \rangle_\alpha$ and $\beta + \langle n^G \rangle_\beta$, respectively; $n \geq 22$ microtubules for each condition; Error bars, S.D; p-value > 0.05 (ns), ≤ 0.05 (*), 0.01 (**), 0.001 (***), 0.0001 (****) by 2-tailed t-test.
(**D**) Reversed phase LC-MS spectra of microtubules first glutamylated by TTLL6 and then glycylated by TTLL3 and used in assays shown in Figure 7H. Throughout, numbers of glutamates and glycines added to α- and β-tubulin are shown in green and magenta/purple, respectively. The weighted mean of glutamates $\langle n^E \rangle$ and glycines $\langle n^G \rangle$ added to α- and β-tubulin (overall and for the separate isoforms) are denoted $\alpha + \langle n^G \rangle_\alpha$ and $\beta + \langle n^G \rangle_\beta$, respectively.
(**E**) Graph showing anti-polyGly antibody signal as a function of Gly number. Glycine numbers determined by LC/MS. Lines, linear regression (black solid line) and 95% confidence interval (grey dotted line); $I = 0.1280 * \langle n^G \rangle_{\alpha\beta}$ where I is anti-polyGly antibody signal; n =3, Error bars, S.D.